Received: 2 January 2025 | Revised: 18 December 2025 | Accepted: 24 December 2025

DOI: 10.1002/esp.70245

RESEARCH ARTICLE

ESPL WILEY

Projected increases in shoreline erosion and potential flooding risk along China's sandy coasts under a warming climate

Xiangfei Li[1] | Shuo Wang[2,3] | Michalis I. Vousdoukas[4] | Mingfu Guan[5] | Wen Dai[1] | Lin Zhao[1]

[1]School of Geographical Sciences, Nanjing University of Information Science & Technology, Nanjing, China

[2]State Key Laboratory of Climate Resilience for Coastal Cities, Department of Land Surveying and Geo-Informatics, The Hong Kong Polytechnic University, Hong Kong, China

[3]Guangdong-Hong Kong Joint Laboratory for Marine Infrastructure, Research Institute for Land and Space, The Hong Kong Polytechnic University, Hong Kong, China

[4]Department of Marine Sciences, University of the Aegean, Mytilene, Greece

[5]Department of Civil Engineering, University of Hong Kong, Hong Kong, China

Correspondence
Shuo Wang, State Key Laboratory of Climate Resilience for Coastal Cities, Department of Land Surveying and Geo-Informatics, The Hong Kong Polytechnic University, Hong Kong.
Email: shuo.s.wang@polyu.edu.hk

Funding information
Hong Kong Polytechnic University, Grant/Award Number: P0056768; National Natural Science Foundation of China, Grant/Award Number: 42501158; the Natural Science Foundation of the Jiangsu Higher Education Institutions of China, Grant/Award Numbers: 22KJB170016, 25KJB170017; the Startup Foundation for Introducing Talent of NUIST, Grant/Award Number: 2024r084

Abstract

Shoreline erosion and coastal flooding are two major hazards causing significant losses of life and property in a warming climate. To enhance coastal resilience against climate change, this study offers an integrated assessment of long-term shoreline erosion (the combined shoreline retreats driven by ambient dynamics and sea level rise) and potential flooding risk (PFR, quantified by the annual cumulative exceedance hours of extreme sea levels) along China's sandy beaches. We further examine the concurrent coastal hazard (CCH) of shoreline erosion and PFR, and evaluate the associated exposure of physical assets and population. Our findings suggest that under the high emission scenario SSP5–8.5, China's sandy beaches are projected to experience intensified erosion and elevated PFRs, primarily attributable to rising mean sea levels. Moreover, shoreline erosion is proportionally more prevalent along the southern coasts. Coastlines projected to experience fewer PFR hours tend to exhibit higher severity, and vice versa. As a result, more than 65% of sandy shorelines are threatened by CCH, and over 80% of coastal physical assets and populations along sandy beaches are exposed to CCH. Among the cities in China's Greater Bay Area, Hong Kong and Shenzhen are projected to face the highest levels of exposure for both physical assets and population. This study identifies future hotspots of shoreline erosion and coastal flooding along China's sandy coastlines and provides scientific evidence to support adaptation strategies aimed at mitigating climate-induced coastal hazards.

KEYWORDS
asset, coastal hazard, exposure, population, vulnerability

1 | INTRODUCTION

The coastline of mainland China stretches 18 000 km across tropical and temperate zones, which is home to a growing population and booming economic activities (Liu & Xing, 2019). The coastal provinces create nearly 60% of national gross domestic product (GDP) with 40% of the population (Cai et al., 2009). Among them, the Guangdong–Hong Kong–Macao Greater Bay Area (GBA) stands out as the country's most dynamic economic cluster and a hub for technological innovation (Li et al., 2021; Textor, 2024; You, Ji, & Bai, 2018). In recent decades, because of the socio-economic development and climate change, China's coastlines are facing a range of pressures such as over-exploitation and sea level rise (Defeo et al., 2009; Wu, Hou, & Xu, 2014). As a result, shoreline erosion and coastal flooding have become increasingly frequent (Fang et al., 2017), threatening both the physical stability of sandy coasts and the ecosystem services they provide (Liu et al., 2021; Paprotny et al., 2021). Recent estimates suggest that shoreline erosion caused 14.3 ha of land recession and ~51.84 million USD losses in China in 2017 (Cao et al., 2022). Coastal flooding has resulted in an annual economic loss of 1.56 billion USD and 49 deaths from 2000 to 2017 (Feng et al., 2018). Notably, the GBA's low terrain, abundant precipitation and dense river network make it highly vulnerable to such coastal hazards (Wang et al., 2024).

Extensive research has assessed coastal erosion and flooding across China (Fang et al., 2021b; Feng et al., 2018; Hou et al., 2016; Li et al., 2023; Xu & Gong, 2018). Approximately 20% of China's

coastlines are considered highly erosion-prone (Cao et al., 2022), primarily owing to sea level rise, sediment reduction and unsustainable coastal exploitation (Cai et al., 2009). Human intervention such as shrimp farming and infrastructure construction has also accelerated shoreline retreat, particularly along the Bohai Sea and southeastern coasts near Shanghai (Mentaschi et al., 2018). At the same time, coastal flooding has increased since the 1980s because of rising extreme sea levels driven mainly by mean sea level rise (Feng et al., 2019; Shi et al., 2015). Variations in storm surges, extreme precipitation and local human activities, such as groundwater extraction and dredging, further intensify flood hazards (Fang et al., 2021a; Feng & Tsimplis, 2014; Pelling, Uehara, & Green, 2013; Tang et al., 2021).

Despite these advances, several research gaps remain. First, existing erosion assessments rarely focus on sandy beaches or quantify the contributions of different erosion drivers, especially under future scenarios. Second, coastal flooding studies usually rely on tide-gauge observations or event-based records and typically evaluate only a subset of total water level components (Fang et al., 2022; Feng et al., 2015, 2019; Li et al., 2024). A holistic understanding of the coastal flooding and the effects of all components of total water level is still lacking. Third, shoreline erosion and coastal flooding frequently co-occur and can mutually reinforce one another (Finkl, 2013). Flooding may trigger or exacerbate erosion (Vousdoukas et al., 2020), while eroded beaches lose their natural buffering capacity and heighten flood vulnerability. Given the emerging interactions between hazards under a warming climate, assessing the concurrent coastal hazards (CCH) of shoreline erosion and flooding is crucial for risk-informed coastal planning.

To address these gaps, this study presents an integrated assessment of projected shoreline erosion and coastal flooding risks along China's sandy beaches. We quantify the contributions of all major erosion and flooding drivers, and evaluate future changes in CCH and associated socio-economic exposures. The research outcomes are expected to provide practical guidance for preparedness, mitigation and adaptation to a wide range of climate extremes and concurrent hazards.

2 | DATA AND METHODS

2.1 | Long-term shoreline erosion of sandy beaches

Long-term shoreline change rate (d_{lt}, m/year) of sandy coasts is quantified following the approach of Vousdoukas et al. (2020):

$$d_{lt} = AC + SR \tag{1}$$

where AC represents ambient shoreline change rate (m/year) driven by natural factors (e.g. hydrodynamic and geological processes) and/or anthropogenic influences (e.g. human activities altering sediment supply or transport). SR is shoreline retreat rate (m/year) owing to sea level rise.

AC is determined as the annual change rate of historical shoreline positions, which are discretised into shoreline points using densely spaced (250 or 500 m) shore-normal transects. Specifically, we use the 32-year (1984–2015) datasets from Luijendijk et al. (2018) and Mentaschi et al. (2018). To minimise local anomalies, a spatial smoothing method is applied to each transect by incorporating all transects from both datasets within a 5-km radius along the same coastal segment. Additionally, AC values are constrained within ±10 m/year to exclude unrealistic outliers. This ensures sufficient data coverage and compensates for missing or low-quality satellite observations. Following Vousdoukas et al. (2020), AC in the future is assumed to be consistent with historical trends.

SR for each transect is estimated based on the Bruun rule (Bruun, 1962):

$$SR = (sea\ level\ rise\ rate)/tan\beta \tag{2}$$

where sea level rise rate is projected from the IPCC Sixth Assessment Report (Garner et al., 2021), and $tan\beta$ is coastal slope derived from a global dataset with a resolution of 1 km along coastlines (Athanasiou et al., 2019).

Finally, shoreline change rates are classified into five types: accretion (> 0.5 m/year), stable (−0.5–0.5 m/year), light erosion ($-1 \sim -0.5$ m/year), intense erosion ($-3 \sim -1$ m/year) and severe erosion (<−3 m/year) (Esteves & Finkl, 1998).

2.2 | Identification of potential flooding risk

Hourly total water level (m) is first calculated as a linear superposition of mean sea level (m), astronomic tide (m), storm surge (m) and wave runup (Fang et al., 2021a; Muis et al., 2018; Song et al., 2020):

$$\begin{aligned} Total\ water\ level = {} & mean\ sea\ level + astronomic\ tide + storm\ surge \\ & + wave\ runup \end{aligned} \tag{3}$$

and wave runup is estimated using the parametrisation of Stockdon et al. (2006):

$$\text{wave runup} = \begin{cases} 0.043\sqrt{H_s L_0}, & \xi < 0.3 \\ 1.1\left(0.35 tan\beta\sqrt{H_s L_0} + 0.5\left[H_s L_0\left(0.5625(tan\beta)^2 + 0.004\right)\right]^{0.5}\right), & \xi \geq 0.3 \end{cases} \tag{4}$$

where $\xi = tan\beta/(H_s/L_0)$ is the Iribarren number, H_s is the significant wave height, $L_0 = 9.8{T_p}^2/2\pi$ is the wavelength of incident wave and T_p is the spectrum peak wave period.

Then, hourly extreme sea levels are identified as events exceeding the 99% percentile of the total water level time series. Potential flooding risk (PFR) is represented by the annual cumulative exceedance hours of extreme sea level. PFR severity is quantified using extreme sea level heights.

In this study, mean sea level, astronomic tide and storm surge are ensemble medians from the Deltares Global Tide and Surge Model (GTSM v3.0) forced by five global climate models (CMCC-CM2-VHR4, EC-Earth3P-HR, GFDL-CM4C192-SST, HadGEM3-GC31-HM and HadGEM3-GC31-HM-SST) (Muis et al., 2022). H_s and T_p are obtained from the First Institute of Oceanography-Earth System Model (FIO-ESM v2.0), which adequately captures wave climate features (Song et al., 2020). All the sea level components cover historical (1980–2014) and future periods (2015–2050, SSP5–8.5), and are resampled to 1-h intervals.

We focus exclusively on SSP5–8.5 because it is the only scenario available from GTSM v3.0 that provides high-resolution sea level data encompassing all key components (i.e. mean sea level, astronomic tide and storm surge). Moreover, the SSP5–8.5 scenario aligns most closely with observed post-2006 emission trends (Chen et al., 2020; Frölicher, Fischer, & Gruber, 2018) and offers a valuable high-end stress test for coastal risk assessment and adaptation planning (Jevrejeva et al., 2023).

2.3 | Exposure of physical asset and population to CCH

Coastline transects experiencing shoreline erosion and a significant ($p < 0.05$) increase in PFR under SSP5–8.5 are identified as CCH hotspots. PRF trends are quantified via Sen's slope estimator, whose statistical significance is tested using Mann–Kendall method.

Exposure of physical asset and population are assessed at the provincial level for mainland China and at the city level within GBA. Physical asset and population distributions are represented by the LitPop dataset (Eberenz et al., 2020) and LandScan 2019 (Rose et al., 2020), respectively, both at 30 arc-second resolutions. Exposure is quantified as

$$\text{exposure} = \sum_{i=1}^{N} r_i \omega_i \quad (5)$$

where N is the number of coastal grid cells, r_i is the fraction of transects within the ith grid exposed to CCH, and ω_i is the physical asset and population in that grid.

3 | RESULTS

3.1 | Assessment and projection of long-term shoreline erosion

Figure 1a shows the projected long-term coastal change rate under SSP5–8.5 by 2050. The mainland China's sandy beaches are expected to experience widespread but spatially heterogeneous shoreline change with an average rate of −0.8 m/year (Figure 1a). Nationally, 65% of sandy beaches are projected to undergo varying degree of erosion at a mean rate of −2.0 m/year, with over 80% of these beaches facing intense or greater erosion (<−1 m/year, Figure 1a and b). In addition, southern provinces exhibit a larger proportion of erosional shorelines, whereas shoreline accretion is proportionally more prevalent along the northern coasts (Figure 1a). Provinces, including Guangdong, Fujian, Shandong, Zhejiang and Liaoning, will have the longest erosional sandy shorelines by 2050 (Figure 1b).

SR explains most of the projected erosion in comparison with AC along mainland China's coastline (68% vs. 32%, Figure 1b). However, AC contributes more prominently to erosion in northern provinces (Figure 1b). In Tianjin, Hebei and Jiangsu, AC accounts for more than 50% of total erosion, consistent with the higher AC rates in these regions (Figure 1c). The weaker SR contribution in northern regions (Figure 1d) is associated with slower local sea level rise (Figure S1a, Supporting Information) and steeper beach slopes (Figure S1b), resulting in a marked north–south contrast in AC and SR contributions (Figure 1b).

Within the GBA, 68% of sandy coasts are projected to retreat, with intense erosion being the dominant category (Figure 2a). Jiangmen, Huizhou, Zhuhai, Hong Kong and Shenzhen rank the top five cities with the longest erosive sandy beaches (Figure 2a). Sandy shoreline erosion in all GBA cities except Dongguan is predominantly driven by sea level rise (Figure 2b), which on average explains ~70% of the overall erosion.

3.2 | Projection of PRF

PFR shows an overall increase under SSP5–8.5 (Figure 3). Historically, PFR occurred for a total of 85.8 h per year on average (Figure 3a). By 2050, this number is expected to rise to 235.0 h annually, representing an average increase of 176.4% (Figure 3b and c). The mean severity of historical PFR is 2.04 m, with a slight yet statistically significant increase to 2.08 m projected for the future, supported by the two-sample t-test (Figure S2). Although PFRs occur less frequently, high-severity events are mainly detected in Jiangsu, Shanghai, Zhejiang and Fujian provinces (Figures 3b and S2b). Coastlines characterised by lower PFR severity are projected to experience more PFR hours, such as those in Bohai Bay, Shandong, eastern Guangdong and Hainan provinces (Figures 3c and S2). In the GBA, historical PFR ranges from 83.6 to 96.7 h with an average of 90.4 h (Figure 3d). Future PFR is expected to increase by 90.8–230.9%, reaching an average of 229.9 h (Figure 3e, f). A slight but significant increase in PFR severity is also projected for the GBA (Figure S3).

We further evaluate the relative contributions of mean sea levels, astronomic tide, storm surge and wave runup (R) to PFR severity (Figure 4a, b). In general, astronomic tide is the dominant contributor, and wave runup plays a secondary but considerable role. In several northern provinces (e.g. Hebei, Tianjin and Shandong), wave runup contributes as much as, or more than, astronomic tide (Figure 4a and Table S1). The contribution of mean sea level, which is negligible historically (Figure 4a), is expected to substantially increase under SSP5–8.5 (Figure 4b). The trends of PFR severity are generally positive, with mean sea level contributing most strongly, especially under SSP5–8.5 (Figure 4c, d and Table S2). Along the South China Sea coast (Guangdong, Guangxi, Hainan, Hong Kong and Macau), however, historical PFR severity shows a negative trend, consistent with that of astronomic tide (Figure 4c). This is potentially associated with the reduced tropical cyclones influence in recent years (Wang & Zhou, 2017). In the GBA, mean sea level plays a negligible historical role but becomes an important contributor in the future (Figures S4a and S4b), considerably influencing both historical and future PFR severity trends (Figure S4c and S4d).

3.3 | Assessment of CCH

Under SSP5–8.5, more than 50% of sandy beaches in most provinces are expected to experience CCH, especially in southern provinces (Figure 5a). Provinces with long coastlines are projected to have extensive sandy beaches affected by CCH (e.g. Guangdong, Fujian, Zhejiang, Shandong and Liaoning). Hotspots of CCH are concentrated along the Liaodong Peninsula, Shandong Peninsula, Qiongzhou

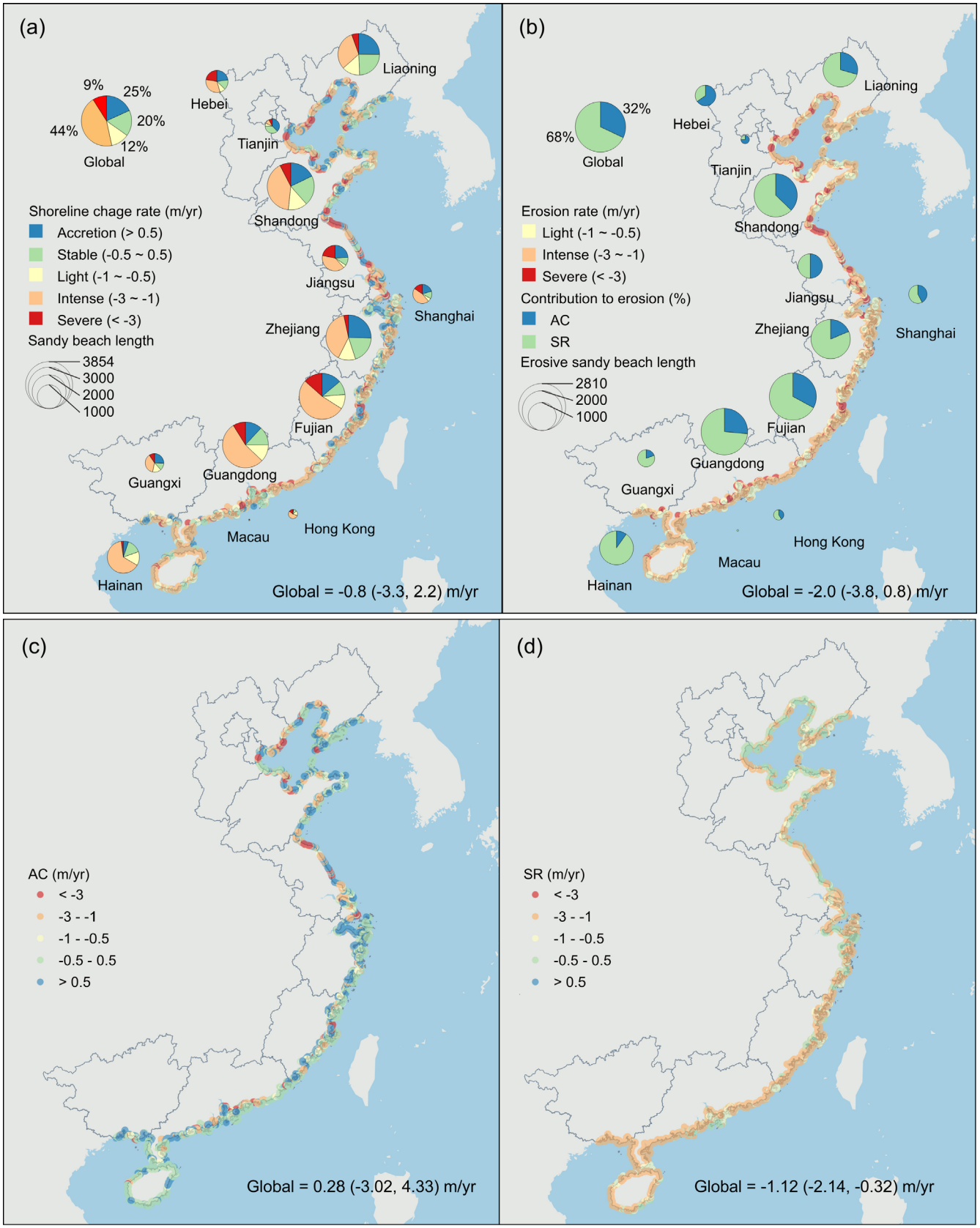

FIGURE 1 Projected long-term (a) shoreline change rate (d_{lt}) and (b) coastal erosion rate by 2050 under SSP5–8.5. Pie charts in Figure 1a show the fractions of five shoreline change types, while those in Figure 1b show the relative contributions (%) of ambient shoreline change rate (AC) and sea-level-rise-driven change (SR) to d_{lt} for each province. The circle size of pie charts indicates the length of sandy or erosive sandy coastlines (transection counts). Figure 1c and d presents AC and SR, respectively. Inset texts give the national mean rate with 5th–95th percentile range.

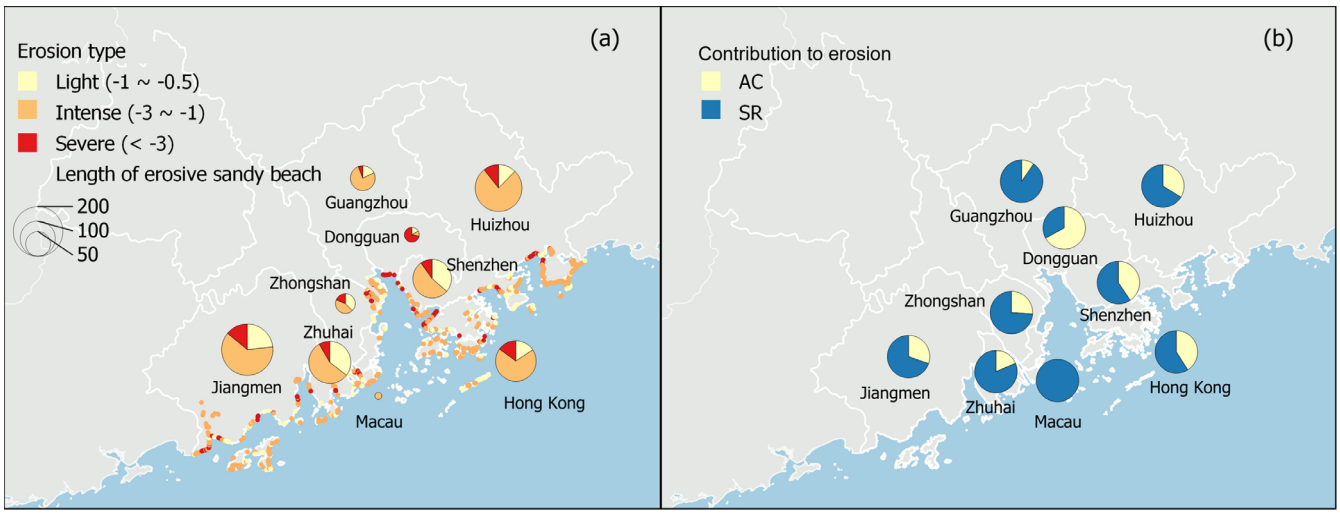

FIGURE 2 (a) Projected long-term coastal erosion rate over the GBA by 2050 under SSP5–8.5. Pie charts show the fraction of three shoreline erosion types for each city, with circle size indicating the length of erosive sandy beach (transection counts). (b) Relative contribution (%) of AC and SR to d_{lt}. GBA, Greater Bay Area; AC, ambient shoreline change rate; SR, shoreline retreat rate.

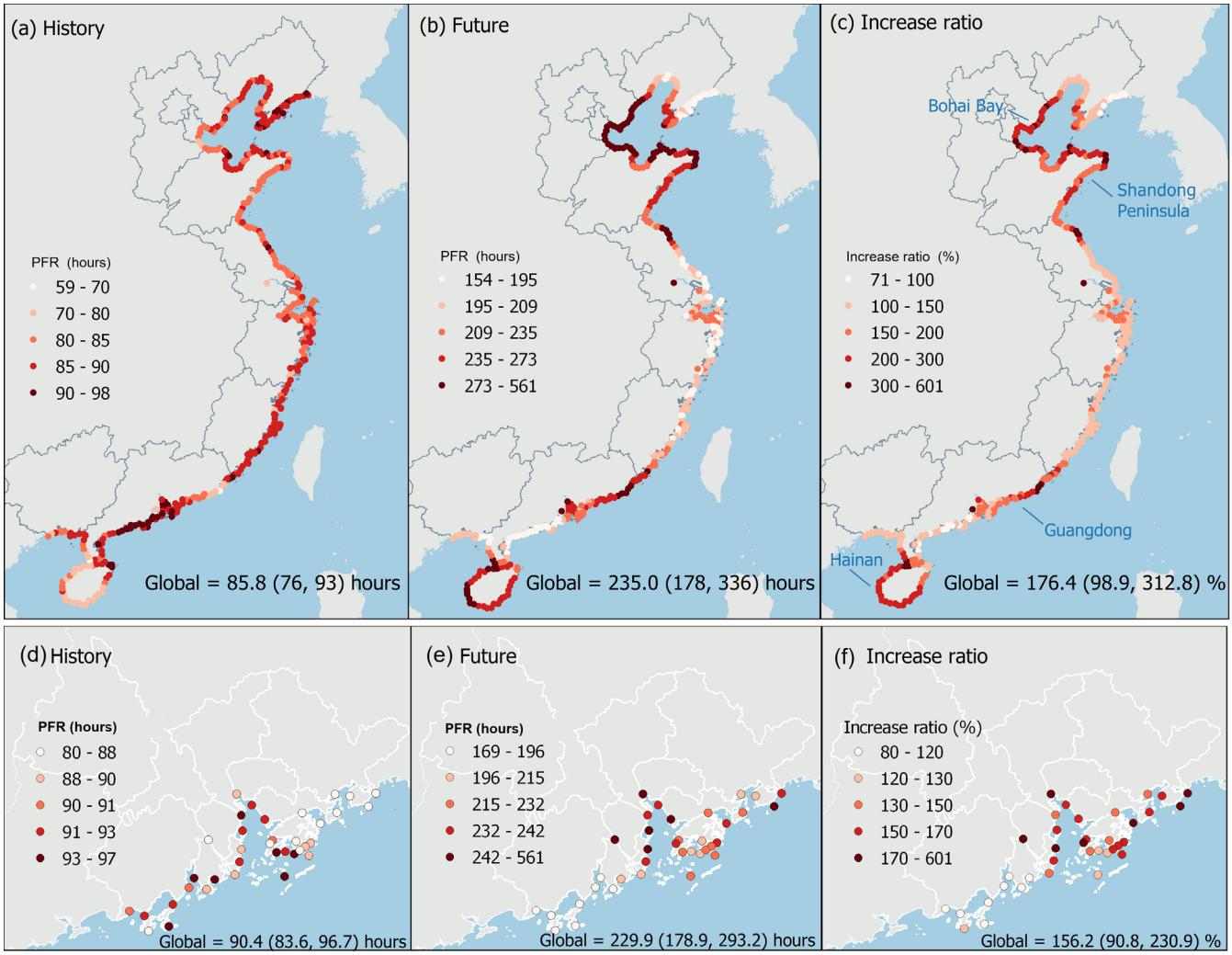

FIGURE 3 (a, d) Historical and (b, e) projected potential flooding risk (PFR) as well as the growth ratio of projected to (c) historical PFR for China's (top row) and GBA's (bottom row) coast by 2050 under SSP5–8.5. The inset texts show the national averages with the 5th–95th percentile range. GBA, Greater Bay Area.

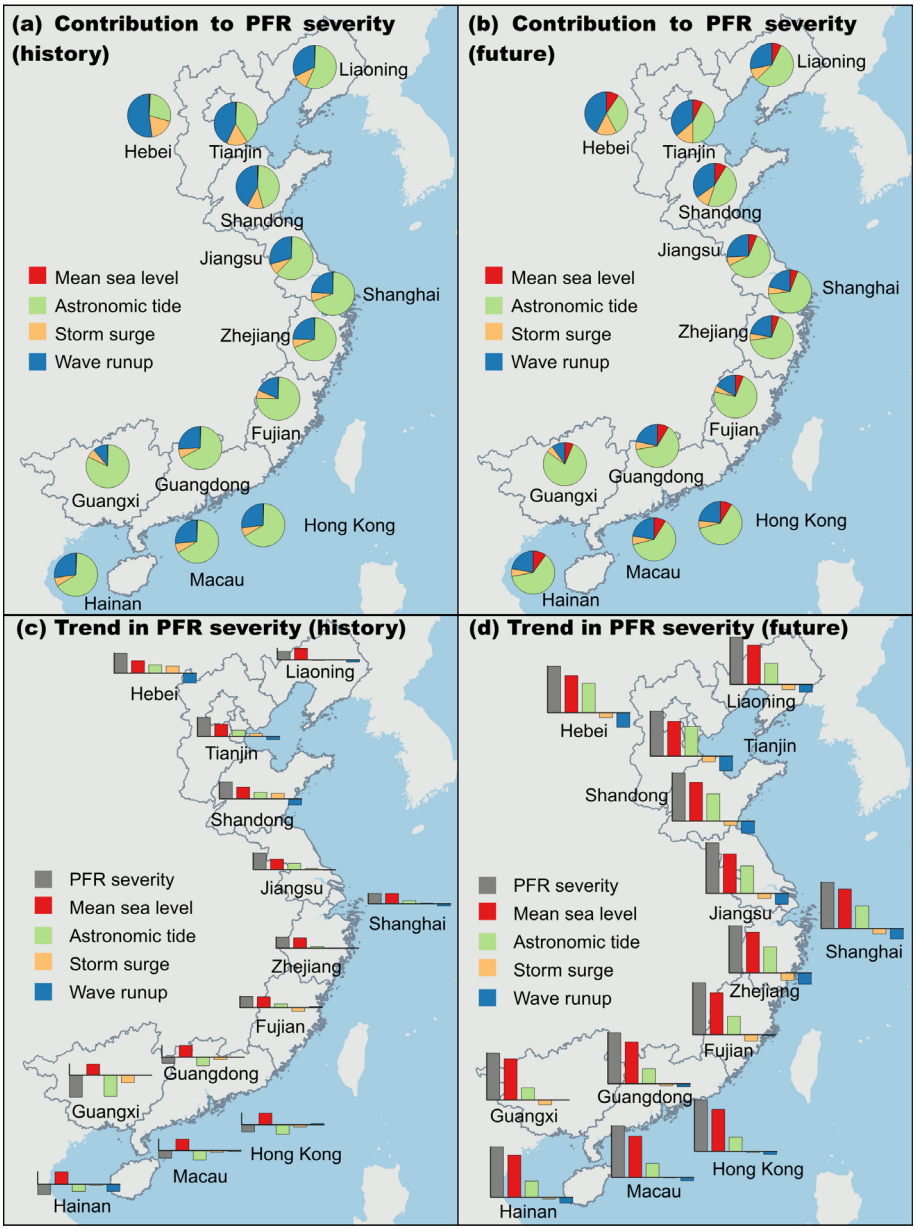

FIGURE 4 Relative contribution (%) of mean sea level (red), astronomic tide (light green), storm surge (orange) and wave runup (blue) to (a, b) PFR severity and to its (c, d) trend. PFR, potential flooding risk.

Peninsula, Pearl River Delta and the coastal areas of Zhejiang and Fujian provinces (Figure 5a).

Most coastal physical assets and population in each province are under the threat of CCH, with a global average fraction of 84% and 88%, respectively. As a result, an estimated 24.93 billion USD in physical assets and 5493 thousand people are exposed to CCH nationwide (Table 1). The exposure shows a pronounced north–south contrast, with significantly higher levels in southern provinces. Guangdong, Fujian, Shanghai and Zhejiang rank highest in both physical assets and population exposure (Figure 5b, c).

Within the GBA, most sandy beaches are expected to be affected by CCH, except in Zhuhai (Figure 5d). Approximately 4736 million USD in physical assets and 401 thousand people are at risk, representing ~19% and ~7% of nationwide exposure, respectively. Shenzhen (~1398 million USD), Hong Kong (~1364 million USD), Macau (~1049 million USD) and Zhuhai (~621 million USD) show the highest physical asset exposure (Figure 5e and Table 2). Population exposure is mainly concentrated in Hong Kong (232 thousand people) and Shenzhen (78 thousand people), together accounting for 77% of exposed populations in the GBA (Figure 5f and Table 2).

4 | DISCUSSION

This study investigates the historical and future coastal hazards, including long-term shoreline erosion, PFR and their concurrence along mainland China's sandy coasts, with particular focus on the GBA. Consistent with previous studies (Vousdoukas et al., 2020; Wu, Hou, & Xu, 2014; Xu & Gong, 2018), we identify a pronounced accretive AC over the past decades, driven by rapid industrialisation and land reclamation (Figure 2a), alongside intensified shoreline erosion in the future forced by sea level rise under SSP5–8.5 scenario (Figure 2b). Our analysis focusses on the long-term erosion. Episodic storm-induced erosion is beyond the scope of this study as it is

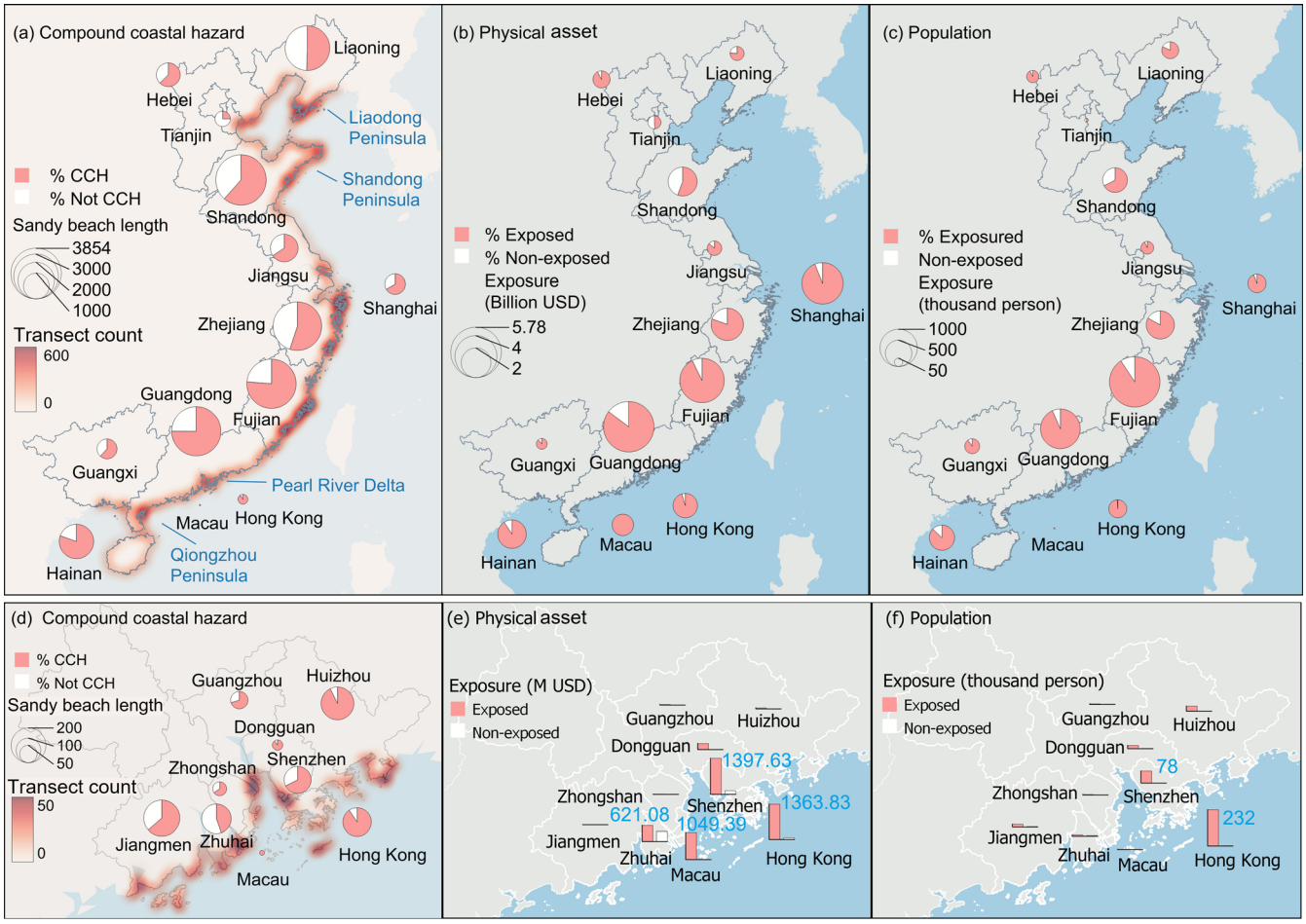

FIGURE 5 (a) Hotspot of concurrent coastal hazard (CCH) of shoreline erosion and PFR. Heat map depicts the density of sandy beaches (transect count) projected to experience the CCH. Pie charts show the fractions of affected (pink) or unaffected (white) sandy beaches, with circle size indicating the length of affected coastlines (transection counts). (b, c) Physical asset and population exposure to CCH. Pie charts show the fractions of exposed (pink) versus unexposed (white) assets or population, with circle size indicating the affected amounts. (d, f) Same as Figure 5a–c but for the GBA. Blue numbers in Figure 5e and f denote the exposed assets and population of the most affected cities. GBA, Greater Bay Area.

usually followed by a recovery process (Ranasinghe, Callaghan, & Stive, 2012; Vousdoukas, Almeida, & Ferreira, 2012). We further identify astronomic tide as the dominant control on PFR severity, followed by wave runup (Figure 4a and b), which is in agreement with observations from other regions (Melet et al., 2018; Serafin, Ruggiero, & Stockdon, 2017). Mean sea level emerges as the dominant factor to the trends in PFR severity (Figure 4c and d), consistent with evidence from tide-gauge records (Feng et al., 2015; Melet et al., 2018).

The majority of sandy coasts are projected to experience CCH, resulting in over 80% of physical assets and population being exposed (Figure 5a–c). Within the GBA, Hong Kong and Shenzhen exhibit the highest exposure of physical assets and population (Figure 5e and f). It should be noted that temporal changes in physical assets and population are not considered in this study. Thus, exposure estimates reflect present-day conditions and are intended to identify regions currently most at risk. As physical assets or population change is likely a key driver of future coastal risk, integrating economic and demographic projections will be essential in future assessments, particularly when linking changes in hazard drivers to climate change (Archer et al., 2024).

Although epistemic uncertainties can be reduced by merging two datasets, the accuracy of AC strongly depends on Landsat-derived shoreline detection accuracy (García-Rubio, Huntley, & Russell, 2015; Hagenaars et al., 2018; Luijendijk et al., 2018; Mentaschi et al., 2018). Additionally, projections of AC are estimated based on historical observations without considering the future dynamics of associated contributors regarding human activities, hydrology or geology (Vousdoukas et al., 2020). While the Bruun rule remains debated (Cooper & Pilkey, 2004; Stive, Ranasinghe, & Cowell, 2009), it continues to serve as a computationally efficient and widely applied approach for large-scale assessments (Brooks & Spencer, 2012; Hinkel et al., 2013; Ranasinghe & Stive, 2009). To enhance its applicability, we adopt high-resolution coastal slopes instead of a constant value used in previous studies (Ardhuin & Roland, 2012; Hinkel et al., 2013; Melet et al., 2018). However, our approach does not account for retreat limited by non-erodible backshore boundaries (Paprotny et al., 2021; Vousdoukas et al., 2022). Similarly, water levels are downscaled to coastal transects via nearest-neighbour interpolation (Depsky et al., 2023; Kirezci et al., 2020), which may introduce uncertainty given the strong dependence of local water levels on coastline geometry, bathymetry, subsidence and ocean dynamics (Nicholls

TABLE 1 Exposure of physical asset and population to CCH for each province of China.

Province	Physical asset (billion USD)		Population (thousand person)	
	Exposed	Non-exposed	Exposed	Non-exposed
Liaoning	0.45 (0.11, 0.31, 0.03)	0.14	206 (79, 117, 10)	45
Hebei	0.67 (0.15, 0.36, 0.16)	0.06	109 (9, 56, 43)	9
Tianjin	0.39 (0.12, 0.26, 0.01)	0.41	10 (5, 5, 0)	10
Shandong	1.91 (0.81, 0.82, 0.28)	1.52	439 (111, 296, 32)	212
Jiangsu	0.48 (0.02, 0.40, 0.05)	0.07	118 (6, 89, 22)	9
Shanghai	3.84 (0.02, 2.71, 1.11)	0.25	239 (20, 153, 65)	15
Zhejiang	2.38 (0.32, 1.39, 0.67)	0.58	569 (131, 423, 15)	115
Fujian	4.50 (0.82, 2.82, 0.86)	0.35	1823 (284, 1,239, 300)	186
Guangdong	5.78 (1.28, 4.10, 0.40)	1.00	1,129 (157, 850, 123)	80
Guangxi	0.27 (0.03, 0.15, 0.09)	0.04	162 (15, 123, 24)	17
Hainan	1.85 (0.19, 1.58, 0.08)	0.19	456 (37, 401, 18)	67
Hong Kong	1.36 (0.20, 0.99, 0.17)	0.06	233 (49, 166, 17)	2
Macau	1.05 (0.00, 1.05, 0.00)	0.00	2 (0, 2, 0)	0
Total	24.93 (4.09, 16.93, 3.91)	4.67	5493 (903, 3919, 671)	767

Note: Values in brackets indicate exposure to CCH under light, intense, and severe erosion scenarios, respectively.
Abbreviation: CCH, concurrent coastal hazard.

TABLE 2 Same as Table 1 but for each city of GBA.

Province	Physical asset (million USD)		Population (thousand person)	
	Exposed	Non-exposed	Exposed	Non-exposed
Dongguan	236.15 (56.51, 37.67, 141.97)	3.14	21 (3, 2, 16)	2
Guangzhou	20.44 (4.55, 13.51, 2.38)	3.43	4 (1, 3, 0)	2
Hong Kong	1363.83 (208.69, 988.97, 166.17)	63.70	232 (49, 166, 17)	2
Huizhou	35.99 (11.67, 21.87, 2.45)	1.60	33 (6, 26, 1)	2
Jiangmen	1.22 (0.41, 0.69, 0.12)	0.21	18 (4, 12, 2)	3
Macau	1049.39 (0.00, 1049.39, 0.00)	0.00	2 (0, 2, 0)	0
Shenzhen	1397.63 (153.48, 1236.54, 7.61)	140.91	78 (15, 59, 4)	0
Zhongshan	10.07 (4.22, 5.00, 0.85)	0.82	3 (1, 2, 0)	0
Zhuhai	621.08 (510.17, 89.83, 21.08)	393.61	9 (3, 5, 1)	5
Total	4735.80 (949.69, 3443.48, 342.63)	607.42	401 (83, 275, 42)	16

Abbreviation: GBA, Greater Bay Area.

et al., 2021; Resio & Westerink, 2008; Woodworth et al., 2019). The effects of existing or planned coastal protection structures (such as dykes and levees) on flooding are also not included because of limited data availability. Our results provide a national-scale overview of future challenges posed by coastal hazards.

5 | CONCLUSIONS

This study assesses the long-term erosion, PFR and the CCHs along China's sandy coastlines, and quantifies the exposure of physical assets and population to the CCHs. Under SSP5–8.5, rising mean sea level is projected to cause widespread and severe erosion, with a typical erosion rate of −3 to −1 m/yr by 2050. Future PFR is also expected to intensify, increasing to 1.76 times that of the historical period on average. As coastal erosion and PFR both worsen, 65% of sandy shorelines in China will be threatened by CCH, and over half of sandy beaches in most provinces, particularly those in the south, are projected to experience CCH. More than 80% of physical assets and population will be exposed to CCH, amounting to a total exposure of 24.93 billion USD and 5.49 million people. The GBA is no exception, with intense future erosion and high PFR, and Hong Kong and Shenzhen are expected to face the greatest exposure among GBA cities. This study will facilitate the preparedness, mitigation and adaptation to a wide range of coastal extremes and contributes to enhancing urban resilience to coastal hazards.

AUTHOR CONTRIBUTIONS

Xiangfei Li and Shuo Wang designed the research. Xiangfei Li performed the research and wrote the manuscript. Michalis I. Vousdoukas, Mingfu Guan, Wen Dai and Lin Zhao contributed data and ideas. All the co-authors revised the manuscript.

ACKNOWLEDGEMENTS

This research is supported by the Hong Kong Polytechnic University (Project No. P0056768), the National Natural Science Foundation of China (grant No. 42501158), the Natural Science Foundation of the Jiangsu Higher Education Institutions of China (Project No. 22KJB170016, 25KJB170017) and the Startup Foundation for Introducing Talent of NUIST (grant No. 2024r084). AI-assisted tools are used solely for language polishing; all scientific content and conclusions are developed by the authors.

CONFLICT OF INTEREST STATEMENT

The authors declare no conflict of interest.

DATA AVAILABILITY STATEMENT

The data of this study are available from the corresponding author upon reasonable request.

ORCID

Xiangfei Li https://orcid.org/0000-0001-6186-3844
Shuo Wang https://orcid.org/0000-0001-7827-187X
Mingfu Guan https://orcid.org/0000-0002-5684-4697
Wen Dai https://orcid.org/0000-0001-7424-644X

REFERENCES

Archer, L., Neal, J., Bates, P., Lord, N., Hawker, L., Collings, T., et al. (2024) Population exposure to flooding in small island developing states under climate change. *Environmental Research Letters*, 19(12), 124020. Available from: https://doi.org/10.1088/1748-9326/ad78eb

Ardhuin, F. & Roland, A. (2012) Coastal wave reflection, directional spread, and seismoacoustic noise sources. *Journal of Geophysical Research, Oceans*, 117, C00J20. Available from: https://doi.org/10.1029/2011JC007832

Athanasiou, P., van Dongeren, A., Giardino, A., Vousdoukas, M., Gaytan-Aguilar, S. & Ranasinghe, R. (2019) Global distribution of nearshore slopes with implications for coastal retreat. *Earth System Science Data*, 11(4), 1515–1529. Available from: https://doi.org/10.5194/essd-11-1515-2019

Brooks, S.M. & Spencer, T. (2012) Shoreline retreat and sediment release in response to accelerating sea level rise: measuring and modelling cliffline dynamics on the Suffolk Coast, UK. *Global and Planetary Change*, 80-81, 165–179. Available from: https://doi.org/10.1016/j.gloplacha.2011.10.008

Bruun, P. (1962) Sea-level rise as a cause of shore erosion. *Journal of the Waterways and Harbors Division*, 88(1), 117–130. Available from: https://doi.org/10.1061/JWHEAU.0000252

Cai, F., Su, X., Liu, J., Li, B. & Lei, G. (2009) Coastal erosion in China under the condition of global climate change and measures for its prevention. *Progress in Natural Science*, 19(4), 415–426. Available from: https://doi.org/10.1016/j.pnsc.2008.05.034

Cao, C., Cai, F., Qi, H., Liu, J., Lei, G., Zhu, K., et al. (2022) Coastal erosion vulnerability in mainland China based on fuzzy evaluation of cloud models. *Frontiers in Marine Science*, 8, 790664. Available from: https://doi.org/10.3389/fmars.2021.790664

Chen, X., Li, N., Zhang, Z., Liu, J. & Wang, F. (2020) Estimation of future global population exposure to heatwaves—based on the heat stress index. *Climate Change Research*, 16(4), 424–432. Available from: https://www.climatechange.cn/EN/Y2020/V16/I4/424

Cooper, J.A.G. & Pilkey, O.H. (2004) Sea-level rise and shoreline retreat: time to abandon the Bruun Rule. *Global and Planetary Change*, 43(3), 157–171. Available from: https://doi.org/10.1016/j.gloplacha.2004.07.001

Defeo, O., McLachlan, A., Schoeman, D.S., Schlacher, T.A., Dugan, J., Jones, A., et al. (2009) Threats to sandy beach ecosystems: a review. *Estuarine, Coastal and Shelf Science*, 81(1), 1–12. Available from: https://doi.org/10.1016/j.ecss.2008.09.022

Depsky, N., Bolliger, I., Allen, D., Choi, J.H., Delgado, M., Greenstone, M., et al. (2023) DSCIM-Coastal v1.1: an open-source modeling platform for global impacts of sea level rise. *Geoscientific Model Development*, 16(14), 4331–4366. Available from: https://doi.org/10.5194/gmd-16-4331-2023

Eberenz, S., Stocker, D., Röösli, T. & Bresch, D.N. (2020) Asset exposure data for global physical risk assessment. *Earth System Science Data*, 12(2), 817–833. Available from: https://doi.org/10.5194/essd-12-817-2020

Esteves, L.S. & Finkl, C.W. (1998) The problem of critically eroded areas (CEA): an evaluation of Florida beaches. *Journal of Coastal Research*, 26, 11–18. Available from: https://www.jstor.org/stable/25736114

Fang, J., Liu, W., Yang, S., Brow, S., Nicholls, R.J., Hinkel, J., et al. (2017) Spatial-temporal changes of coastal and marine disasters risks and impacts in Mainland China. *Ocean and Coastal Management*, 139, 125–140. Available from: https://doi.org/10.1016/j.ocecoaman.2017.02.003

Fang, J., Nicholls, R.J., Brown, S., Lincke, D., Hinkel, J., Vafeidis, A.T., et al. (2022) Benefits of subsidence control for coastal flooding in China. *Nature Communications*, 13(1), 6946. Available from: https://doi.org/10.1038/s41467-022-34525-w

Fang, J., Wahl, T., Fang, J., Sun, X., Kong, F. & Liu, M. (2021a) Compound flood potential from storm surge and heavy precipitation in coastal China: dependence, drivers, and impacts. *Hydrology and Earth System Sciences*, 25(8), 4403–4416. Available from: https://doi.org/10.5194/hess-25-4403-2021

Fang, J., Wahl, T., Zhang, Q., Muis, S., Hu, P., Fang, J., et al. (2021b) Extreme sea levels along coastal China: uncertainties and implications. *Stochastic Environmental Research and Risk Assessment*, 35(2), 405–418. Available from: https://doi.org/10.1007/s00477-020-01964-0

Feng, J., Li, D., Wang, T., Liu, Q., Deng, L. & Zhao, L. (2019) Acceleration of the extreme sea level rise along the Chinese coast. *Earth and Space Science*, 6(10), 1942–1956. Available from: https://doi.org/10.1029/2019EA000653

Feng, J., Li, H., Li, D., Liu, Q., Wang, H. & Liu, K. (2018) Changes of extreme sea level in 1.5 and 2.0°C warmer climate along the coast of China. *Frontiers in Earth Science*, 6, 216. Available from: https://doi.org/10.3389/10.3389/feart.2018.00216

Feng, J., von Storch, H., Jiang, W. & Weisse, R. (2015) Assessing changes in extreme sea levels along the coast of China. *Journal of Geophysical Research, Oceans*, 120(12), 8039–8051. Available from: https://doi.org/10.1002/2015JC011336

Feng, X. & Tsimplis, M.N. (2014) Sea level extremes at the coasts of China. *Journal of Geophysical Research, Oceans*, 119(3), 1593–1608. Available from: https://doi.org/10.1002/2013JC009607

Finkl, C.W. (Ed). (2013) *Coastal hazards*. Dordrecht, The Netherlands: Springer. Available from: https://doi.org/10.1061/9780784412664

Frölicher, T.L., Fischer, E.M. & Gruber, N. (2018) Marine heatwaves under global warming. *Nature*, 560(7718), 360–364. Available from: https://doi.org/10.1038/s41586-018-0383-9

García-Rubio, G., Huntley, D. & Russell, P. (2015) Evaluating shoreline identification using optical satellite images. *Marine Geology*, 359, 96–105. Available from: https://doi.org/10.1016/j.margeo.2014.11.002

Garner, G. G., Hermans, T., Kopp, R. E., Slangen, A. B. A., Edwards, T. L., Levermann, A., et al. (2021) Sea level projections from the IPCC 6th Assessment Report (AR6). Physical Oceanography Distributed Active Archive Center (PODAAC).

Hagenaars, G., de Vries, S., Luijendijk, A.P., de Boer, W.P. & Reniers, A.J.H.M. (2018) On the accuracy of automated shoreline detection derived from satellite imagery: a case study of the sand motor mega-scale nourishment. *Coastal Engineering*, 133, 113–125. Available from: https://doi.org/10.1016/j.coastaleng.2017.12.011

Hinkel, J., Nicholls, R.J., Tol, R.S.J., Wang, Z.B., Hamilton, J.M., Boot, G., et al. (2013) A global analysis of erosion of sandy beaches and sea-level rise: an application of DIVA. *Global and Planetary Change*, 111, 150–158. Available from: https://doi.org/10.1016/j.gloplacha.2013.09.002

Hou, X., Wu, T., Hou, W., Chen, Q., Wang, Y. & Yu, L. (2016) Characteristics of coastline changes in mainland China since the early 1940s. *Science China Earth Sciences*, 59(9), 1791–1802. Available from: https://doi.org/10.1007/s11430-016-5317-5

Jevrejeva, S., Williams, J., Vousdoukas, M.I. & Jackson, L.P. (2023) Future sea level rise dominates changes in worst case extreme sea levels along the global coastline by 2100. *Environmental Research Letters*, 18(2), 024037. Available from: https://doi.org/10.1088/1748-9326/acb504

Kirezci, E., Young, I.R., Ranasinghe, R., Muis, S., Nicholls, R.J., Lincke, D., et al. (2020) Projections of global-scale extreme sea levels and resulting episodic coastal flooding over the 21st century. *Scientific Reports*, 10(1), 11629. Available from: https://doi.org/10.1038/s41598-020-67736-6

Li, C., Ng, M.K., Tang, Y. & Fung, T. (2021) From a 'world factory' to China's Bay Area: a review of the outline of the development plan for the Guangdong-Hong Kong-Macao Greater Bay Area. *Planning Theory and Practice*, 23(2), 310–314. Available from: https://doi.org/10.1080/14649357.2021.1958539

Li, S., Wahl, T., Fang, J., Liu, L. & Jiang, T. (2023) High-tide flooding along the China coastline: Past and future. Earth's. *Futures*, 11(4), e2022EF003225. Available from: https://doi.org/10.1029/2022EF003225

Li, W., Wang, H., Xiang, W., Wang, A., Xu, W., Jiang, Y., et al. (2024) Sea-level change in coastal areas of China: status in 2021. *Advances in Climate Change Research*, 15(3), 515–524. Available from: https://doi.org/10.1016/j.accre.2024.06.002

Liu, C., Yang, M., Hou, Y. & Xue, X. (2021) Ecosystem service multi-functionality assessment and coupling coordination analysis with land use and land cover change in China's coastal zones. *Science of the Total Environment*, 797, 149033. Available from: https://doi.org/10.1016/j.scitotenv.2021.149033

Liu, D. & Xing, W. (2019) Analysis of China's coastal zone management reform based on land-sea integration. *Marine Economics and Management*, 2(1), 39–49. Available from: https://doi.org/10.1108/MAEM-03-2019-0001

Luijendijk, A., Hagenaars, G., Ranasinghe, R., Baart, F., Donchyts, G. & Aarninkhof, S. (2018) The state of the world's beaches. *Scientific Reports*, 8(1), 6641. Available from: https://doi.org/10.1038/s41598-018-24630-6

Melet, A., Meyssignac, B., Almar, R. & Le Cozannet, G. (2018) Under-estimated wave contribution to coastal sea-level rise. *Nature Climate Change*, 8(3), 234–239. Available from: https://doi.org/10.1038/s41558-018-0088-y

Mentaschi, L., Vousdoukas, M.I., Pekel, J.-F., Voukouvalas, E. & Feyen, L. (2018) Global long-term observations of coastal erosion and accretion. *Scientific Reports*, 8(1), 12876. Available from: https://doi.org/10.1038/s41598-018-30904-w

Muis, S., Apecechea, M. I., Álvarez, J. A., Verlaan, M., Yan, K., Dullaart, J., et al. (2022) Global sea level change time series from 1950 to 2050 derived from reanalysis and high resolution CMIP6 climate projections. Copernicus Climate Change Service (C3S) Climate Data Store (CDS). Available from: https://doi.org/10.24381/cds.a6d42d60

Muis, S., Haigh, I.D., Guimarães Nobre, G., Aerts, J.C.J.H. & Ward, P.J. (2018) Influence of El Niño-Southern Oscillation on global coastal flooding. *Earth's Future*, 6(9), 1311–1322. Available from: https://doi.org/10.1029/2018EF000909

Nicholls, R.J., Lincke, D., Hinkel, J., Brown, S., Vafeidis, A.T., Meyssignac, B., et al. (2021) A global analysis of subsidence, relative sea-level change and coastal flood exposure. *Nature Climate Change*, 11(4), 338–342. Available from: https://doi.org/10.1038/s41558-021-00993-z

Paprotny, D., Terefenko, P., Giza, A., Czapliński, P. & Vousdoukas, M.I. (2021) Future losses of ecosystem services due to coastal erosion in Europe. *Science of the Total Environment*, 760, 144310. Available from: https://doi.org/10.1016/j.scitotenv.2020.144310

Pelling, H., Uehara, K. & Green, J.M. (2013) The impact of rapid coastline changes and sea level rise on the tides in the Bohai Sea, China. *Journal of Geophysical Research: Oceans*, 118(7), 3462–3472. Available from: https://doi.org/10.1002/jgrc.20258

Ranasinghe, R., Callaghan, D. & Stive, M.J.F. (2012) Estimating coastal recession due to sea level rise: beyond the Bruun rule. *Climatic Change*, 110(3), 561–574. Available from: https://doi.org/10.1007/s10584-011-0107-8

Ranasinghe, R. & Stive, M.J.F. (2009) Rising seas and retreating coastlines. *Climatic Change*, 97(3), 465–468. Available from: https://doi.org/10.1007/s10584-009-9593-3

Resio, D.T. & Westerink, J.J. (2008) Modeling the physics of storm surges. *Physics Today*, 61(9), 33–38. Available from: https://doi.org/10.1063/1.2982120

Rose, A., McKee, J., Sims, K., Bright, E., Reith, A. & Urban, M. (2020) *LandScan Global 2019*. Oak Ridge National Laboratory, Oak Ridge, TN: LandScan Global. Available from: https://doi.org/10.48690/1524214

Serafin, K.A., Ruggiero, P. & Stockdon, H.F. (2017) The relative contribution of waves, tides, and nontidal residuals to extreme total water levels on U.S. West Coast sandy beaches. *Geophysical Research Letters*, 44(4), 1839–1847. Available from: https://doi.org/10.1002/2016GL071020

Shi, X., Liu, S., Yang, S., Liu, Q., Tan, J. & Guo, Z. (2015) Spatial–temporal distribution of storm surge damage in the coastal areas of China. *Natural Hazards*, 79(1), 237–247. Available from: https://doi.org/10.1007/s11069-015-1838-z

Song, Z., Bao, Y., Zhang, D., Shu, Q., Song, Y. & Qiao, F. (2020) Centuries of monthly and 3-hourly global ocean wave data for past, present, and future climate research. *Scientific Data*, 7(1), 226. Available from: https://doi.org/10.1038/s41597-020-0566-8

Stive, M.J.F., Ranasinghe, R. & Cowell, P. (2009) Sea level rise and coastal erosion. In: Kim, Y. (Ed.) *Handbook of coastal and ocean engineering*, Singapore: World Scientific, pp. 1023–1037. Available from: https://doi.org/10.1142/9789812819307_0037

Stockdon, H.F., Holman, R.A., Howd, P.A. & Sallenger, A.H. (2006) Empirical parameterization of setup, swash, and runup. *Coastal Engineering*, 53(7), 573–588. Available from: https://doi.org/10.1016/j.coastaleng.2005.12.005

Tang, W., Zhan, W., Jin, B., Motagh, M. & Xu, Y. (2021) Spatial variability of relative sea-level rise in Tianjin, China: insight from InSAR, GPS, and tide-gauge observations. *IEEE Journal of Selected Topics in Applied Earth Observations and Remote Sensing*, 14, 2621–2633. Available from: https://doi.org/10.1109/JSTARS.2021.3054395

Textor, C. (2024) Greater Bay Area in China - statistics & facts. Statista, https://www.statista.com/topics/5333/greater-bay-area-in-china/#topicOverview

Vousdoukas, M.I., Almeida, L.P.M. & Ferreira, Ó. (2012) Beach erosion and recovery during consecutive storms at a steep-sloping, meso-tidal beach. *Earth Surface Processes and Landforms*, 37(6), 583–593. Available from: https://doi.org/10.1002/esp.2264

Vousdoukas, M.I., Clarke, J., Ranasinghe, R., Reimann, L., Khalaf, N., Duong, T.M., et al. (2022) African heritage sites threatened as sea-level rise accelerates. *Nature Climate Change*, 12(3), 256–262. Available from: https://doi.org/10.1038/s41558-022-01280-1

Vousdoukas, M.I., Ranasinghe, R., Mentaschi, L., Plomaritis, T.A., Athanasiou, P., Luijendijk, A., et al. (2020) Sandy coastlines under threat of erosion. *Nature Climate Change*, 10(3), 260–263. Available from: https://doi.org/10.1038/s41558-020-0697-0

Wang, W. & Zhou, W. (2017) Statistical modeling and trend detection of extreme sea level records in the Pearl River Estuary. *Advances in Atmospheric Sciences*, 34(3), 383–396. Available from: https://doi.org/10.1007/s00376-016-6041-y

Wang, Y., Liu, C., Wang, Y., Liu, Y. & Liu, T. (2024) Climate risk assessment and adaption ability in China's coastal urban agglomerations—a case study of Guangdong-Hong Kong-Macao greater bay area. *Journal of Cleaner Production*, 452, 142036. Available from: https://doi.org/10.1016/j.jclepro.2024.142036

Woodworth, P.L., Melet, A., Marcos, M., Richard, D.R., Guy, W., Yoshi, N.S., et al. (2019) Forcing factors affecting sea level changes at the coast. *Surveys in Geophysics*, 40(6), 1351–1397. Available from: https://doi.org/10.1007/s10712-019-09531-1

Wu, T., Hou, X. & Xu, X. (2014) Spatio-temporal characteristics of the mainland coastline utilization degree over the last 70 years in China. *Ocean and Coastal Management*, 98, 150–157. Available from: https://doi.org/10.1016/j.ocecoaman.2014.06.016

Xu, N. & Gong, P. (2018) Significant coastline changes in China during 1991–2015 tracked by Landsat data. *Scientific Bulletin*, 63(14), 883–886. Available from: https://doi.org/10.1016/j.scib.2018.05.032

You, Z.-J., Ji, Z. & Bai, Y. (2018) Impacts of storm wave-induced coastal hazards on the coast of China. *Journal of Coastal Research*, 85(s1), 826–830. Available from: https://doi.org/10.2112/SI85-166.1

SUPPORTING INFORMATION

Additional supporting information can be found online in the Supporting Information section at the end of this article.

How to cite this article: Li, X., Wang, S., Vousdoukas, M.I., Guan, M., Dai, W. & Zhao, L. (2026) Projected increases in shoreline erosion and potential flooding risk along China's sandy coasts under a warming climate. *Earth Surface Processes and Landforms*, 51(1), e70245. Available from: https://doi.org/10.1002/esp.70245